Sticking coefficient for atoms scattering on metallic surfaces

Celso R. C. Rêgo,[1,2,3,4,*] Ryan Requist,[1,5] Axel Schild,[6] E. K. U. Gross,[1,5] and Luiz N. Oliveira[2]

[1] *Max-Planck Institut für Mikrostruturphysik, Weinberg 2, D-06120 Halle, Germany*
[2] *São Carlos Institute of Physics, University of São Paulo, 13560-970, São Carlos, Brazil*
[3] *Karlsruhe Institute of Technology (KIT), Institute of Nanotechnology, 76344 Eggenstein-Leopoldshafen, Germany*
[4] *Amazonas State University, Av. Djalma Batista 3578, Flores, 69050-010, Manaus, Brazil*
[5] *Fritz Haber Center for Molecular Dynamics, Institute of Chemistry, The Hebrew University, Jerusalem 91904, Israel*
[6] *ETH Zürich, Laboratorium für Physikalische Chemie, 8093 Zürich, Switzerland*

(Dated: March 30, 2025)

Achieving a complete understanding of the quantum dynamical processes arising when an atom approaches a metallic surface remains a key challenge in surface physics. Conventional approaches based on the Born-Oppenheimer approximation become inapplicable when charge is transferred between the surface and the adatom and the resulting image-charge potential accelerates the particle toward the surface. Here, we solve the time-dependent Schrödinger equation to compute the electronic contribution to the sticking coefficient for a generalized version of the Anderson-Newns Hamiltonian and obtain adsorption probabilities as large as 15%. Numerical simulations demonstrate that the creation of low-energy electron-hole pairs is an efficient dissipation mechanism that may absorb enough kinetic energy from the incident particle to cause adsorption. The recently proposed exact factorization formalism affords a physical interpretation of the results.

Keywords: sticking coefficient

INTRODUCTION

The study of dynamical processes is among the most active frontiers in physics and chemistry. Examples of atomic-scale processes are the interaction of intense laser fields with molecules, the scattering of electrons from atoms and small molecules, and the collision of molecules or atoms against metallic surfaces [1–5]. In all of them, the Born-Oppenheimer (BO) approximation may fail when the nuclear motion couples electronic states separated by small energy gaps.

In the collision of a hydrogen atom against a metallic surface, particle-hole excitations across the Fermi level define arbitrarily small energy differences. The BO potential energy surfaces (PES) form a continuum. An additional difficulty comes from the image-charge potential, which causes rapid nuclear motion that renders the BO approximation inapplicable and bars perturbative treatment of the non-adiabatic coupling terms (NACT) [4, 6, 7]. Notwithstanding the large body of work dedicated to such collisions, the physics of ion-surface charge and energy transfer remains poorly understood, and previous theoretical work [8, 9] has shown that adiabatic and classical pictures are inadequate.

From the experimental perspective, non-adiabatic effects have long been associated with energy dissipation in molecular or atomic collisions against metallic surfaces [10–13]. The notion that electron-hole excitations are a source of dissipation underpins a number of early theoretical works [14, 15] as well as molecular-dynamics studies in which a density-friction approximation describes the loss of translational energy [13, 16–21]. Thus, we believe that an accurate treatment must encompass a quantum mechanical description of the nuclear motion and its correlation with the electron dynamics.

Typically, the BO approximation is used to separate the electronic degrees of freedom from the nuclear dynamics, which can then be described by a time-dependent Schrödinger equation (TDSE) with a *static* PES. However, the importance of going beyond this adiabatic approximation in calculations of the sticking coefficient was pointed out long ago [22–25]. Introducing the concept of a time-dependent potential energy surface (TDPES) allows one to describe nonadiabatic dynamics [26–28]. Abedi *et al.* [26, 27] have shown that the *exact factorization* formalism puts that concept on a solid foundation and provides a rigorous separation of the electronic and nuclear equations of motion.

Here, we present a numerical computation of the *sticking coefficient*, or adsorption probability, for a hydrogen atom impinging upon a solid metal. We will show that the exact factorization formalism offers physical insight into the processes leading to adsorption.

To compute sticking coefficients, one must face two conceptual challenges. First, one must adequately describe the electronic structure of the atom-surface system, including electron transfer and electron-electron correlations. The second challenge is describing the dynamics of the metallic surface electrons under the influence of the moving H atom or ion, which generates a time-dependent potential that excites electron-hole pairs. The dynamics take place on multiple time scales, including the charge transfer time, the transit time through the nonadiabatic coupling region, and the arbitrarily long time scale of electron-hole excitation/de-excitation.

To surmount the first obstacle, we introduce a generalized Anderson-Newns Hamiltonian and treat the conduction band continuum via a logarithmically discretized

set of single-particle states, as introduced in the numerical renormalization group (NRG) approach [29–31]. To tackle the second, we diagonalize the discretized Hamiltonian, which incorporates the rapid dynamics of the conduction electrons, and then rely on an accurate numerical procedure to integrate the TDSE of the composite atom-surface system. Assisted by the exact factorization formalism, we infer the nuclear wavefunction and the TDPES describing the backreaction of the excited metal on the atomic motion. The sticking coefficient is determined from the fraction of the nuclear wave packet that is found at a relatively short distance from the surface in the long time limit.

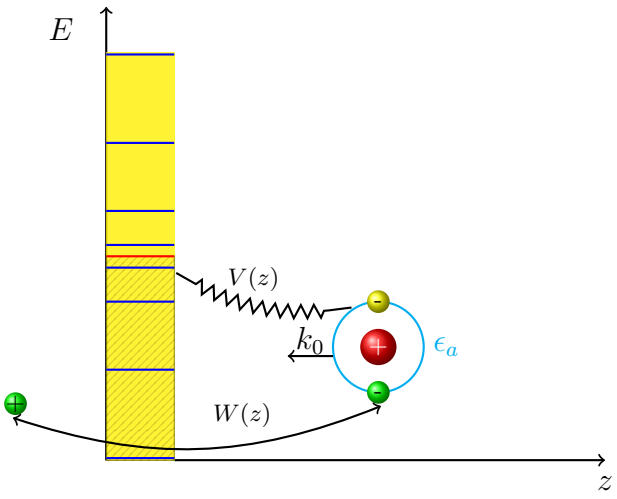

FIG. 1. (Color online). Surface-adatom scattering model defined by Eq. (1). A single level, with energy ϵ_a, represents the H atom, at the position z relative to the surface. The yellow rectangle depicts the structureless conduction band representing the metal. Far from the surface (large z), the atomic level is occupied by a single electron and does not interact with the conduction band. Closer to the surface (small z), the coupling $V(z)$ allows one electron to be transferred from one of the conduction states to the H level. The ionization of the adatom switches on the momentum-independent image-charge potential $W(z)$.

Figure 1 depicts the interactions in the system. We consider normal incidence of the atom upon the surface. Far from the surface, the minute overlap between the atomic and metallic wavefunctions impedes transitions between them. The hydrogen proton and electron therefore move as a bound pair toward the metal. Closer to the surface, the overlap grows. Eventually, electronic hopping between the metal and the atomic orbital becomes possible. As the atom approaches the surface the coupling becomes strong, and the atom tends to become negatively ionized and is attracted to the surface by its image charge. Electron-hole and phonon excitations in the ensuing collision dissipate energy [9, 10, 13, 32], and the ion may not have enough energy to overcome the image-charge potential and move away from the surface. Our focus is on electron-hole excitations, and their contribution to the sticking coefficient.

An extension of the Anderson-Newns Hamiltonian models our system. The metal nuclei are fixed, and a single nuclear coordinate, the distance z between the hydrogen proton and the surface, appears in the model Hamiltonian, which reads

$$H = \sum_k \epsilon_k c_k^\dagger c_k + \epsilon_a n_a + U n_{a\uparrow} n_{a\downarrow} + V(z)(f_0^\dagger c_a + \text{H.c.}) - W(z) f_0^\dagger f_0 (n_a - 1)^2 + \frac{P_z^2}{2M} \quad (1)$$

with implicit spin sums.

The first term on the right-hand side of Eq. (1) is a structureless noninteracting, half-filled conduction band of width $2D$, which represents the metallic electrons. The Fermi operator c_a annihilates an electron at the hydrogen orbital, and the Fermi operator f_0 is a shorthand for $(1/\sqrt{N})\sum_k c_k$, where N denotes the number of conduction-band levels.

The second and third terms on the right-hand side of Eq. (1) define the hydrogen Hamiltonian. The atomic level ϵ_a and Coulomb repulsion U are chosen to reproduce the experimental energies $-13.6\,\text{eV}$ and $-14.4\,\text{eV}$ for singly (H) and doubly occupied (H^-) hydrogen, respectively. Choosing the zero of energy to be the Fermi energy of the conduction band of a metal, e.g. Cu, with work function $4.6\,\text{eV}$ gives $\epsilon_a = -9.0\,\text{eV}$ and $U = 12.8\,\text{eV}$. The fourth term on the right-hand side couples the metallic states to the hydrogen level. To represent the decay of the coupling with the distance from the surface, we choose $V(z) = A\exp(-az)$. The prefactor A will be defined below, while the inverse range a is a free parameter. The fifth term, where $W(z) \equiv 1/[4(z - z_{im})]$, represents the image-charge potential [33], which is turned on upon ionization ($n_a : 1 \to 2$). The coupling prefactor $A = 3.5\,\text{eV}$ and the position of the image-charge plane $z_{im} = -1.3\,\text{Bohr}$ were chosen to approximately reproduce the adsorption energy ($2.4\,\text{eV}$) of H on Cu(111) as calculated by density functional theory [34].

To allow numerical treatment of the electronic degrees of freedom, we substitute the discretized NRG series $\sum_{n=0}^{N-1} t_n(f_n^\dagger f_{n+1} + \text{H. c.})$ for the first term on the right-hand side of Eq. (1), a controllable approximation that yields essentially exact results [30]. The coefficients t_n ($n = 0, \ldots, N$) are proportional to the half-bandwidth D with proportionality coefficients that depend on the discretization parameter Λ [35]; $t_n \approx D\Lambda^{-n/2}$ within deviations of $\mathcal{O}(\Lambda^{-n})$. Standard convergence tests [30] targeting computation of the sticking coefficient with less than 1% deviation showed that $\Lambda = 1.8$ with $N = 11$ adequately represent the continuum ($\Lambda \to 1$, $N \to \infty$) limit.

Our computation starts out with the diagonalization of the BO Hamiltonian, equivalent to the sum of the first five terms on the right-hand side of Eq. (1). We work

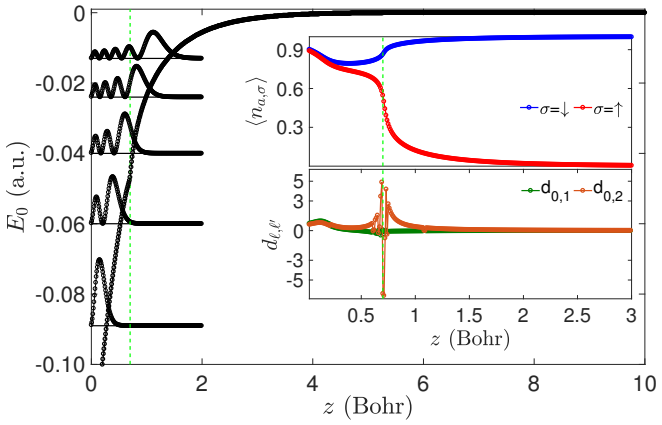

FIG. 2. (Color online). Ground-state potential energy surface [filled circles] and the lowest six vibrational levels [horizontal black lines and open circles] as a function of the nuclear position z. The top inset (blue and red lines) shows the occupations ($\langle n_{a,\sigma}\rangle$, $\sigma =\uparrow,\downarrow$) of the electronic orbital $c_{a,\sigma}$ as functions of position. The bottom inset (orange and dark-green lines) presents the first order non-adiabatic coupling terms $d_{\ell,\ell'} = \langle\Phi_z(\ell)\,|\partial_z\Phi_z(\ell')\rangle$. The dashed green line marks the location of the crossover, where the spin polarization rapidly changes.

within the segment $0 \le z \le z_{\rm M}$, henceforth called *box*, and represent the box, of size $z_{\rm M} = 10\,$Bohr, by a mesh with M equally spaced points. To reduce the computational effort, we adopt the mean-field approximation detailed in the Supplemental Material for the third and fifth terms on the right-hand side of Eq. (1).

The quality of the mean-field approximation depends on the model parameters and energy scale. As discussed in the Supplemental Material, the parameters in our computation make the approximation very reliable over most of the box and less accurate over a small segment, smaller than 10% of the box size. Given that this is the chief source of error in our procedure, we estimate the relative deviation in the calculated sticking coefficients to be of the order of 10% for any initial kinetic energy of the adatom.

The mean-field approximation reduces the BO Hamiltonian to a quadratic form, easily diagonalizable at each position z. The resulting electronic eigenvalues E_ℓ form the BO potential energy surfaces (PES). In our approach, the corresponding eigenstates — Slater determinants $|\phi_\ell\rangle$ of the single-particle states resulting from the diagonalization of the mean-field BO Hamiltonian for $z = z_i$ $(i = 1,\ldots,M)$ — constitute a basis upon which we project the wavefunction $\Psi(z,r,t)$ to solve the time-dependent Schrödinger equation.

Figure 2 shows the ground-state BO PES, measured with respect to its $z \to \infty$ limit. Far from the surface, the atomic orbital is decoupled from the metal, and the atom is neutral. The PES coincides with the energy ϵ_a of the atomic level plus the ground-state energy of the conduction band. For smaller z, hybridization with the metallic levels becomes possible, the hydrogen electronic charge grows, and the image-charge potential pulls down the PES. As the top inset panel shows, there is a crossover at $z = z_c \approx 0.7\,$Bohr to a strong-coupling regime where the hybridization becomes strong enough to couple the $n_a = 2$ and the two $n_a = 1$ configurations ($\uparrow$ and $\downarrow$) of the H level. The crossover at z_c is marked by near degeneracies that enhance the matrix elements of the NACT's, as the bottom inset in Fig. 2 shows.

To solve the time-dependent Schrödinger equation, we use the Crank-Nicolson procedure, an unconditionally stable, highly accurate algorithm that preserves the normalization of the wavefunction [36, 37]. The initial state of the system $|\chi,\phi,t=0\rangle$ is the tensor product of the electronic ground state $|\phi_{\ell=0}\rangle$ and the initial nuclear state $|\chi_{t=0}\rangle$. The wavefunction of the $|\phi_{\ell=0}\rangle$ state is the Slater determinant constructed from the eigenfunctions of the mean-field BO Hamiltonian with eigenvalues below the Fermi level. The initial nuclear state $|\chi_{t=0}\rangle$ is represented by the gaussian wavefunction $\chi(z,0) = B\exp(-(z-z_0)^2/2\xi^2)\exp(-ik_0z)$, centered at $z = z_0$, with spatial width ξ, normalization factor B, and initial momentum k_0. The box size $z_{\rm M}$ is large enough to ensure that $\int_0^{z_{\rm M}}\chi|(z,0)|^2\,{\rm d}z = 1$, with insignificant deviation. The Crank-Nicolson procedure determines $|\chi,\phi,t\rangle$ for $t > 0$.

To guarantee convergence of the procedure, we have examined the evolution of the wavefunction for different numbers of BO surfaces, grid points, and time steps. On the basis of the results, we include 10 BO surfaces in the calculation and use the time step $\delta t = 0.000\,12\,$fs in all computations reported in Figs. 3 and 4 below.

To avoid reflection of the wavefunction at $z = z_{\rm M}$, an absorbing potential (Supp. Mat.) was applied to the interval $z_{\rm M} - \bar{z} \le z \le z_{\rm M}$, with $\bar{z} = 0.8\,$Bohr. The sticking coefficient S was computed as $S = \int_0^{z_{\rm M}}|\chi(z,t_f)|^2\,{\rm d}z$. Given that the integral $\int_0^{z_{\rm M}}|\chi(z,t)|^2\,{\rm d}z$ remains practically constant for $t > 500\,$fs, we have set $t_f = 500\,$fs.

Figure 3 exhibits the dependence of the sticking coefficient on the initial kinetic energy of the incident particle and the inverse range a of the coupling $V(z)$ between the atomic and metallic levels. Tuning a gives insight into how the sticking coefficient varies from atom to atom and surface to surface, depending e.g. on the different spatial extent of the valence orbital. As one would have expected, the sticking coefficient generally decreases with increasing initial kinetic energy. In contrast, dependence on the coupling range shows more structure. The sticking coefficient tends to grow with the range, but the rise is non-monotonic and the oscillations depend on the initial kinetic energy. For the lowest energy ($E_{\rm i} = 0.2\,$eV), there are large fluctuations with the sticking coefficient dropping from 18% to 4% between the maximum at $a = 0.54\,{\rm Bohr}^{-1}$ and the local minimum at $a = 0.62\,{\rm Bohr}^{-1}$. The horizontal undulation across the

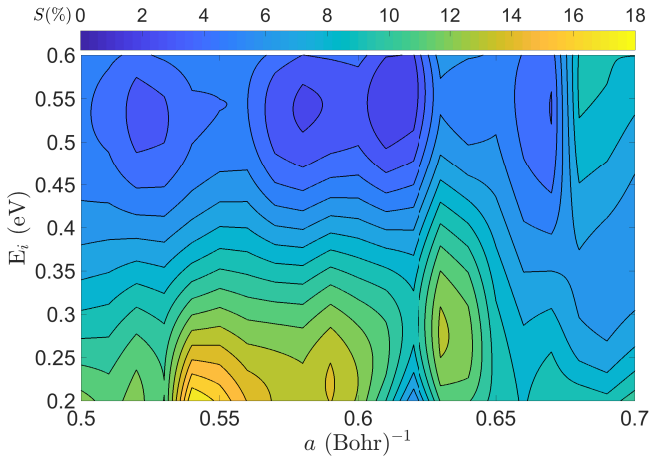

FIG. 3. (Color online). Sticking coefficient as a function of the initial kinetic energy $E_{\rm i}$ (eV) and the decay constant a of the hybridization potential $V(z) = A\exp(-az)$. The colorbar represents the sticking coefficient S for an initially neutral H atom impinging on a metallic surface at normal incidence. All the calculations of this figure were performed with $M = 1000$ grid points.

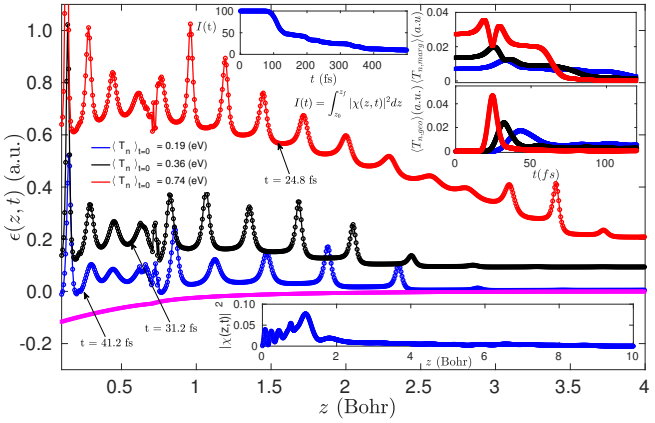

FIG. 4. (Color online). Snapshots of the TDPES, Eq. (3), at the time when the total kinetic energy T_n is maximum. The blue, black and red lines represent different initial kinetic energies $E_{\rm i} = T_n|_{t=0}$. The blue lines in the bottom and top center insets are the remaining nuclear density, $|\chi(z,t)|^2$, after 498 fs of simulation, and the integral $I(t)$, respectively. The upper right insets represent the time evolution of the marginal, $T_{n,marg}$ (upper), and geometric, $T_{n,geo}$ (bottom), contributions to the kinetic energy, respectively. All the calculations of this figure were performed with $M = 1500$ grid points, $\xi = 0.775$ Bohr, and $a = 0.6\,\text{Bohr}^{-1}$. The reference magenta line is the ground-state BOPES.

figure, most easily seen from afar, reflects the dependence on a of the NACT matrix elements responsible for energy transfer between the nucleus and the conduction band, which oscillate in the crossover region and are small elsewhere. The dependence of the sticking coefficient on $E_{\rm i}$ is controlled by a competition between time scales, as discussed next. More work is needed to specify the origin of the structure in quantitative detail.

To further elucidate the real-time quantum dynamics of the collision, we turn to the exact factorization formalism [26], which writes the wavefunction as a single product

$$\Psi(z,r,t) = \chi(z,t)\Phi_z(r,t), \tag{2}$$

where r denotes the electronic coordinates. Both wavefunctions on the right-hand side of Eq. (2) are normalized. In particular $\int |\Phi_z(r,t)|^2\,\mathrm{d}r = 1$, at all times t and for all nuclear positions z.

The nuclear wavefunction $\chi(z,t)$ obeys a TDSE, which in our notation reads

$$\left[\frac{1}{2M}(P_z + A_z)^2 + \epsilon(z,t)\right]\chi(z,t) = i\partial_t\chi(z,t). \tag{3}$$

Here, $A_z = \mathrm{Re}\langle\Phi|P_z\Phi\rangle$ and $\epsilon(z,t)$ is the TDPES of the exact factorization formalism, which has proven useful in studies of isolated molecules [26–28, 38–41]. The metal-adsorbate system under consideration extends the application of the TDPES to cases where the electronic states form a continuum, as also done in a recent study of laser-induced desorption at surfaces [42]. After determining the wavefunction $\Psi(z,r,t)$ via the Crank-Nicolson procedure, we calculate the nuclear function $\chi(z,t)$, choose a gauge such that $A_z = 0$ and invert Eq. (3) to determine $\epsilon(z,t)$; details are given in the Supplemental Material.

Figure 4 shows snapshots of the TDPES at the instant of maximal "squashing" (defined below) of the nuclear wavepacket against the metal surface for three different initial incidence energies. All TDPES's are significantly different from the ground state BOPES (magenta curve) and display spikes whose positions correlate with the z-values where $|\chi(z,t)|^2$ has minima. These minima result from (incomplete) destructive interference between incident and reflected waves. For each curve, the spikes tower above a smooth background potential barrier that rises as the initial kinetic energy $T_n|_{t=0}$ grows (we have computed TDPES's for several $T_n|_{t=0}$ in the interval $[0.19-1.36]$eV to verify this trend). For the smallest initial kinetic energy (blue curve), the low barrier arrests the nuclear wavefunction in the small-z region long enough to allow energy transfer to the low-energy electronic degrees of freedom. On the other hand, the high barrier (~ 0.7 a.u.) for the largest initial kinetic energy (red curve) rapidly repels the atom from the surface, resulting in a nearly perfect elastic collision.

The elasticity vs. inelasticity of the collision is clearly visible in the difference between the nuclear kinetic energy $T_n = \langle\Psi|\frac{1}{2M}P_z^2|\Psi\rangle$ and the partial kinetic energy $T_{n,marg} = \langle\chi|\frac{1}{2M}(P_z + A_z)^2|\chi\rangle$, evaluated with the nuclear wavefunction and the kinetic energy operator in Eq. (3). We refer to this quantity as the geometric part, $T_{n,geo}$, of the nuclear kinetic energy, since it can be writ-

ten as a tensor contraction involving the Fubini-Study metric measuring distance in projective Hilbert space [43]. Since $T_{n,geo}$ is the $|\chi|^2$-weighted integral of the non-negative scalar $\langle\partial_z\Phi_z|\partial_z\Phi_z\rangle$ (for $A_z = 0$), it only vanishes for an unentangled state $|\Psi\rangle$.

The lower panel of the upper right inset in Fig. 4 shows the time evolution of $T_{n,geo}$ for three initial kinetic energies. In each case, $T_{n,geo}$ vanishes at $t = 0$, since the nuclear and electronic degrees of freedom are initially unentangled. As the atom approaches the surface, $T_{n,geo}$ grows and reaches a maximum. We have used this peak, which coincides with the maximum of T_n, to identify the instant of maximal "squashing" of the nuclear wavefunction $\chi(z,t)$ against the metal surface. For each initial kinetic energy, this is the instant for which we display the TDPES in the main plot of Fig. 4. At these instants the hydrogen atom is trying to access all possible energy scales. For the highest initial kinetic energy (red curve), the peak in $T_{n,geo}$ is nearly symmetric, indicating an elastic collision and approximately reversible dynamics: the electronic excitations that build up as the atom approaches the surface are able to "unwind" after the atom abruptly changes direction and propagates away, effectively reversing time as seen by the electrons and hence nearly returning the electronic system to its ground state in the long-time limit.

On the other hand, the asymmetry of $T_{n,geo}$ for lower initial kinetic energies (black and blue curves) is evidence of inelasticity and irreversible energy dissipation. The persistent long-time tail of $T_{n,geo}$ is due to the adsorbed component of the wave function, for the contribution of the outgoing (reflected) wavepacket falls off rapidly as it moves farther away from the surface. As the incidence energy is decreased, the peak in $T_{n,geo}$ broadens substantially, demonstrating that energy is being exchanged between atomic motion and electronic excitations over a progressively longer period of time. An estimate of this time interval is obtained from the full width at half maximum of $T_{n,geo}$, yielding 28, 20, and 8 fs for incidence energies $E_i = 0.19$, 0.36, and 0.74 eV, respectively. These times can be compared with the charge transfer time $\hbar/\Gamma \approx 4.5$ fs, where Γ is the width of the atomic level due to its coupling to the conduction band. While all electronic states are populated at the moment of impact, the long-time behavior is due to low-energy electron-hole pairs, which is similar to x-ray absorption in metals [44, 45]. The real-time BO populations for the full time interval of the simulations are available in the Suppl. Mat.

The top center inset in Fig. 4 shows that, even under the favorable slow-incidence condition defining the blue curves in the figure, the ion has substantial probability to leak out after initial trapping. Nonetheless, the probability-density plot in the bottom inset shows that, after nearly 600 fs, there is nearly 10% trapping probability in this case.

In summary, we have computed the electronic contribution to the adsorption probability following the collision of a H atom with a metallic surface described by a general Anderson-Newns Hamiltonian. Projection of the electronic degrees of freedom onto the NRG basis allows accurate treatment of electron-hole excitations. The sizeable adsorption probabilities obtained show that the creation of such excitations is an efficient dissipative mechanism that absorbs translational energy and ultimately traps the hydrogen ion in the vicinity of the surface.

Axel Schild is grateful for financial support from an Ambizione grant of the Swiss National Science Foundation (SNF). Celso Rêgo's work was partially supported by a CAPES fellowship. This work received financial support from the European Research Council (ERC) under the European Union's Horizon 2020 research and innovation programme (grant agreement no. ERC-2017-AdG-788890) and from CNPq grant no. 312239/2018-1. We thank Ingo Barth, Kunlong Liu computing resources and Udo Schmidt for computing support.

* Correspondent author:celso.rego@kit.edu

[1] A. Schild and E. Gross, Phys. Rev. Lett. **118** (2017), 10.1103/physrevlett.118.163202.
[2] I. Gainullin and M. Sonkin, Comput. Phys. Commun. **188**, 68 (2015).
[3] Y. Huang, C. T. Rettner, D. J. Auerbach, and A. M. Wodtke, Science **290**, 111 (2000).
[4] A. J. Coffman and J. E. Subotnik, Phys. Chem. Chem. Phys. **20**, 9847 (2018).
[5] H. Kono, Y. Sato, N. Tanaka, T. Kato, K. Nakai, S. Koseki, and Y. Fujimura, Chemical Physics **304**, 203 (2004).
[6] F. Martin, J. Fernandez, T. Havermeier, L. Foucar, T. Weber, K. Kreidi, M. Schoffler, L. Schmidt, T. Jahnke, O. Jagutzki, A. Czasch, E. P. Benis, T. Osipov, A. L. Landers, A. Belkacem, M. H. Prior, H. Schmidt-Bocking, C. L. Cocke, and R. Dorner, Science **315**, 629 (2007).
[7] W. Dou and J. E. Subotnik, J. Chem. Phys. **148**, 230901 (2018).
[8] F. J. Bonetto, M. A. Romero, A. Iglesias-García, R. A. Vidal, and E. C. Goldberg, J. Phys. Chem. C **119**, 3124 (2015).
[9] H. Schlichting, D. Menzel, T. Brunner, W. Brenig, and J. C. Tully, Phys. Rev. Lett. **60**, 2515 (1988).
[10] M. Lindenblatt and E. Pehlke, Phys. Rev. Lett. **97** (2006), 10.1103/physrevlett.97.216101.
[11] B. Kasemo, Surf. Sci. **363**, 22 (1996).
[12] T. Greber, Surf. Sci. Rep. **28**, 1 (1997).
[13] O. Bunermann, H. Jiang, Y. Dorenkamp, A. Kandratsenka, S. M. Janke, D. J. Auerbach, and A. M. Wodtke, Science **350**, 1346 (2015).
[14] G. P. Brivio, Physical Review B **35**, 5975 (1987).
[15] K. Schönhammer and O. Gunnarsson, Physical Review B **22**, 1629 (1980).
[16] J. R. Trail, D. M. Bird, M. Persson, and S. Holloway, J. Chem. Phys. **119**, 4539 (2003).
[17] A. Kandratsenka, H. Jiang, Y. Dorenkamp, S. M. Janke,

M. Kammler, A. M. Wodtke, and O. Bünermann, Proc. Natl. Acad. Sci. USA **115**, 680 (2018).
[18] Y. Dorenkamp, C. Volkmann, V. Roddatis, S. Schneider, A. M. Wodtke, and O. Bünermann, J. Phys. Chem. C **122**, 10096 (2018).
[19] Y. Dorenkamp, H. Jiang, H. Köckert, N. Hertl, M. Kammler, S. M. Janke, A. Kandratsenka, A. M. Wodtke, and O. Bünermann, J. Chem. Phys. **148**, 034706 (2018).
[20] J. T. Kindt, J. C. Tully, M. Head-Gordon, and M. A. Gomez, The Journal of Chemical Physics **109**, 3629 (1998).
[21] J. I. Juaristi, M. Alducin, R. D. Muiño, H. F. Busnengo, and A. Salin, Physical Review Letters **100** (2008), 10.1103/physrevlett.100.116102.
[22] J. Nørskov and B. Lundqvist, Surface Science **89**, 251 (1979).
[23] B. Lundqvist, O. Gunnarsson, H. Hjelmberg, and J. Nørskov, Surface Science **89**, 196 (1979).
[24] G. Brivio and T. Grimley, Surface Science **89**, 226 (1979).
[25] R. Brako and D. Newns, Vacuum **32**, 39 (1982).
[26] A. Abedi, N. T. Maitra, and E. K. U. Gross, Phys. Rev. Lett. **105** (2010), 10.1103/physrevlett.105.123002.
[27] A. Abedi, N. T. Maitra, and E. K. U. Gross, J. Chem. Phys. **137**, 22A530 (2012).
[28] A. Abedi, F. Agostini, Y. Suzuki, and E. K. U. Gross, Phys. Rev. Lett. **110** (2013), 10.1103/physrevlett.110.263001.
[29] K. G. Wilson, Rev. Mod. Phys. **47**, 773 (1975).
[30] H. Krishna-murthy, J. Wilkins, and K. Wilson, Phys. Rev. B **21**, 1003 (1980).
[31] L. N. Oliveira and J. W. Wilkins, Phys. Rev. B **24**, 4863 (1981).
[32] B. Gergen, H. Nienhaus, W. H. Weinberg, and E. W. McFarland, Science **294**, 2521 (2001).
[33] P. M. Echenique and J. B. Pendry, Journal of Physics C: Solid State Physics **8**, 2936 (1975).
[34] J. Greeley and M. Mavrikakis, J. Phys. Chem. B **109**, 3460 (2005).
[35] V. L. Campo and L. N. Oliveira, Physical Review B **72** (2005), 10.1103/physrevb.72.104432.
[36] J. Crank, P. Nicolson, and D. R. Hartree, Mathematical Proceedings of the Cambridge Philosophical Society **43**, 50 (1947).
[37] Z. Sun and W. Yang, J. Chem. Phys. **134**, 041101 (2011).
[38] F. Agostini, A. Abedi, Y. Suzuki, and E. Gross, Molecular Physics **111**, 3625 (2013).
[39] Y. Suzuki, A. Abedi, N. T. Maitra, and E. K. U. Gross, Physical Chemistry Chemical Physics **17**, 29271 (2015).
[40] S. K. Min, F. Agostini, and E. Gross, Physical Review Letters **115** (2015), 10.1103/physrevlett.115.073001.
[41] T. Fiedlschuster, J. Handt, E. K. U. Gross, and R. Schmidt, Physical Review A **95** (2017), 10.1103/physreva.95.063424.
[42] E. Boström, A. Mikkelsen, and C. Verdozzi, Phys. Rev. B **93** (2016), 10.1103/physrevb.93.195416.
[43] R. Requist, F. Tandetzky, and E. K. U. Gross, Physical Review A **93** (2016), 10.1103/physreva.93.042108.
[44] P. Nozières and C. T. De Dominicis, Physical Review **178**, 1097 (1969).
[45] J. Friedel, Comments Solid State Phys. **2**, 21 (1969).